Numerical Simulation of Inclined Jets in a Crossflow Using a Reynolds Stress Model

L.S. Jansson [1] and L. Davidson [2]

Abstract. The paper presents a finite-volume calculation procedure employing a second-order closure turbulence model. A collocated variable arrangement is used in combination with the third-order accurate QUICK discretization scheme for the convective terms. Calculated results of the three-dimensional turbulent flow generated by an inclined jet issuing from a circular outlet in a wall into a free stream along this wall are shown. Simulated mean velocity profiles and the adiabatic film-cooling effectiveness are compared to hot-wire measurements. Two different turbulence models are compared: the standard $k-\varepsilon$ model, and a full Reynolds Stress Model (RSM). In order to describe the viscous effects on the turbulence near the walls, a one-equation model by Norris and Reynolds in combination with a mixing layer approach is used.

1 INTRODUCTION

Turbulent flows similar to jets in a crossflow can be found in a number of engineering applications, such as the cooling of gas turbines and combustion chambers, and are of great interest. The thermal efficiency of gas turbines can be improved by higher temperatures at the inlet to the turbine section. Higher temperatures require better cooling methods in order to protect the turbine blades from the hot gases, and hence increase the lifetime of the gas turbine. One such cooling method which is attracting attention, is discrete-hole film-cooling or effusion cooling, in which low-temperature secondary fluid is supplied via several holes within the blade leading to the blade surface, thereby forming a protective film of coolant flow. Intuitively, the cooling will be more effective if the jet bends over and attaches immediately to the surface downstream the jet discharge, and also, the mixing between the cool fluid and the free stream should be small in order to delay the dilution of the cool fluid. As in other film-cooling methods, the extent of the region that should be protected is strongly affected by the jet penetration and mixing with the hot main stream. Such systems must therefore be designed with care.

Some of the parameters that govern the film-cooling effectiveness is the number of holes, the relative hole spacing s/D, the injection angle α, the blowing rate between the jet flow and the main stream $M = \rho_j U_j / \rho_o U_o$, and the diameter D of the injection hole, see Fig. 1.

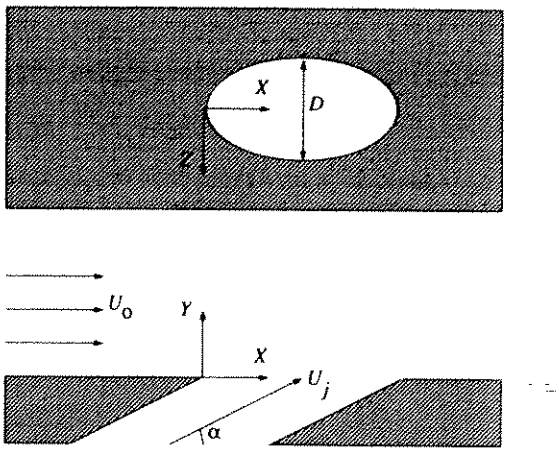

Figure 1. Flow configuration.

It is primarily these parameters that have to be optimized in the design process. The influence of most of these parameters have been experimentally studied separately, mainly for injection of jets into the boundary layer on flat plates. Compilations of measurements of such jets in crossflows can be found in Andreopoulos *et al.* [1], Bergeles *et al.* [2] [3] and Afejuku *et al.* [4]. However, experimental parameter studies at realistic conditions would not only be difficult but also quite expensive and hence there is a great need for valid simulation techniques.

Numerical simulations of jets in crossflows have also been made in recent years and some of them can be found in Claus *et al.* [5], Kim *et al.* [6] and Ince *et al.* [7], but generally, the agreement with measurements is quite poor, especially when the ratio of jet to cross-

[1] Dept. of Thermo and Fluid Dynamics, Chalmers University of Technology, S-412 96 Gothenburg, Sweden
[2] Dept. of Thermo and Fluid Dynamics, Chalmers University of Technology, S-412 96 Gothenburg, Sweden

ECCOMAS 94.
Published in 1994 by John Wiley & Sons, Ltd.

stream velocity is high (M≥1). It is established that, at high velocity ratios, the near field of jets in a crossflow is controlled largely by complex inviscid dynamics so that the influence of turbulence on the flow development is rather limited. However, the flow further downstream is always influenced by turbulence, and at small velocity ratios even the near field is turbulence-dominated. A correct description of the turbulent stresses and heat or mass fluxes are important to complete the picture, and hence a realistic modelling of these quantities is needed, especially in the complex situation of a jet in a crossflow.

In some of the earlier numerical simulations, the upstream region of the jet was excluded from the computational domain. However, Ince *et al.* [7] showed that the distortion of the jet by the crossflow across the jet-discharge plane is an important factor. The usual practice of prescribing a uniform jet discharge velocity profile, due to lack of experimental data, is therefore inappropiate, especially at low ratios of M. A better approch is to incorporate parts of the duct leading to the jet exit into the calculation domain. It is shown in this study that the jet discharge velocity profiles are far from being uniform.

The present work is part of an ongoing project to develop a method for predicting reacting flow in combustion chambers including effusion cooled walls. In this study, a 3D isothermal Reynolds stress model as well as the standard $k-\epsilon$ model have been used in combination with a one-equation model in the near-wall region. The second-moment-closure adopted is that of Gibson and Launder [8]. A two-layer model is used, which combines the turbulence model in the high Reynolds number region with a simpler, but more reliable one-equation model [9] in order to accurately resolve the flow near solid walls. The flow field is divided into an outer region, where the viscous effects are small, and an inner region. This viscous-affected inner region, which includes the sublayer, the buffer layer and part of the fully turbulent layer, is resolved with the one-equation model. The turbulence model used in the high Reynolds number region is matched with the one-equation model at some location in the fully turbulent layer. The implementation was done in a finite volume code CALC-BFC (Boundary - Fitted - Coordinates) [10], based on SIMPLEC and a collocated arrangement and is briefly discussed below. In the momentum equations, the third-order accurate QUICK discretization scheme is used, and in the transport equations for the turbulent quantities, a second-order accurate bounded scheme by van Leer [11] is used.

The flow field properties that are considered in this study are the mean velocities and the adiabatic film-cooling effectiveness for different ratios of M=0.2−1.0 at an injection angle α=30° through a plane wall. The simulations are compared to the measurements by Bergeles *et al.* [3].

2 THE REYNOLDS STRESS MODEL

The time-averaged Reynolds stress transport equation can be written as:

$$\underbrace{\frac{\partial}{dx_k}(\rho U_k \overline{u_i u_j})}_{convection} = \underbrace{-\rho\overline{u_i u_k}\frac{\partial U_j}{dx_k} - \rho\overline{u_j u_k}\frac{\partial U_i}{dx_k}}_{production} + \Phi_{ij} + D_{ij} - \rho\varepsilon_{ij} \quad . \tag{1}$$

The convection and production terms are exact and do not need any modelling assumptions. The modelling of the pressure-strain correlation is done in a standard manner desribed by Gibson and Launder [8]. The diffusion of stresses is described using the eddy viscosity concept and the viscous dissipation is assumed to be isotropic.

3 NEAR-WALL TREATMENT

The one-equation model chosen in this investigation is the one proposed by Norris and Reynolds [9]. The standard transport equation for the turbulent kinetic energy k is solved as usual, but the dissipation rate ε in the near-wall region is explicitly determined from a prescribed length-scale distribution. The model is based on the eddy viscosity concept and in the inner region, the eddy viscosity ν_t and the dissipation rate ε are given as:

$$\nu_t = c_\mu \, k^{1/2} \, \ell_\mu \; ; \qquad \varepsilon = \frac{k^{3/2}}{\ell_\varepsilon} \tag{2}$$

Close to a wall the turbulent energy k decreases, owing to the damping of the turbulent stresses, and hence the eddy viscosity goes to zero. The damping of the eddy viscosity in this inner region is prescribed by a reduction of ℓ_μ, due to an exponential function similar to the van Driest damping function used in the mixing length theory. The turbulent length scales are prescribed as:

$$\ell_\mu = C_\ell \, n \left[1 - exp\left(-\frac{Re_n}{A_\mu} \right) \right] \tag{3}$$

$$\ell_\varepsilon = \frac{C_\ell \, n}{1 + 5.3/Re_n} \tag{4}$$

$$Re_n = \frac{k^{1/2} n}{\nu} \; ; \qquad C_\ell = \kappa \, C_\mu^{-3/4}$$

where n is the normal distance from the wall. The damping constant A_μ is determined from numerical tests and set to A_μ=50.5 [12].

The one-equation model in the inner region must be matched with the high Reynolds number model in the outer region at some location in the flow. In this study, the matching takes place where the damping function in the length-scale relation Eq. (3), i.e. the expression in brackets, has a value close to unity, which means that the viscous effects are small. For the present calculations a value of 0.95 is chosen which corresponds to $Re_n \approx 200$.

4 NUMERICAL IMPLEMENTATION

A decoupling problem may arise when second-order-closure models are used in connection with collocated variable arrangement. In order to stabilize the solution procedure, an apparent diffusion technique is often used which is described by by Huang and Leschziner [13]. However, in the present study, the *maximum* value of the turbulent (or eddy) viscosity μ_t and the apparent viscosity μ_{app} is used in the diffusive term as a stabilising effect and the whole contribution from the Reynolds stresses to the diffusive transport is put into the constant part of the source term. The contribution from the turbulent viscosity μ_{turb} to the diffusion is then subtracted from the source term. As an example, consider the corresponding diffusion in a one-dimensional case for the velocity component in the streamwise direction, U in Fig. 2. The diffusion and the source term can then be written as:

$$DIFF_e = \frac{\mu_{eff} A_e}{\delta x_e} (U_E - U_P) \qquad (5)$$

$$DIFF_w = \frac{\mu_{eff} A_w}{\delta x_w} (U_P - U_W) \qquad (6)$$

where

$$\mu_{eff} = \mu_{lam} + \mu_{turb} \; ; \qquad \mu_{turb} = max\left[\mu_t, \mu_{app}\right]$$

$$S_C^U = S_C^U + \frac{\partial}{\partial x}\left(-\rho\overline{u^2}\right)\delta V - \left[\frac{\mu_{turb} A_e}{\delta x_e}(U_E - U_P) - \frac{\mu_{turb} A_w}{\delta x_w}(U_P - U_W)\right]$$

The corresponding terms in the other two dimensions are similarly derived. The implementation is easy and straightforward, especially in a code in which the $k-\varepsilon$ model already exists, and at least for this particular case, this method turned out to be more stable compared to the apparent diffusion technique by Huang and Leschziner [13]. Another advantage compared to the method by Huang and Leschziner is that the apparent viscosity $\mu_{app,ij}$, which is a second-order tensor, does not need to be transformed between different coordinate systems (from a Cartesian coordinate system to a general non-orthogonal coordinate system along the grid lines), see Ref. [14].

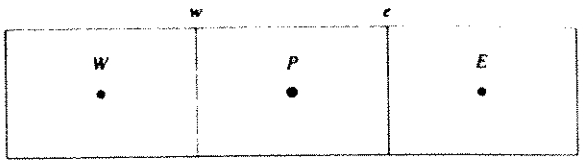

Figure 2. One dimensional case.

5 RESULTS AND DISCUSSION

Numerical three-dimensional simulations of a circular jet entering a free stream at an injection angle α=30° have been done. A selection of the predicted profiles of streamwise mean velocities and adiabatic film-cooling effectiveness Θ at various positions in the flow field are presented for the velocity ratios M=0.2, 0.5 and 1.0. The validity of the simulations are compared to the measurements by Bergeles *et al.* [3]. It should be noted that the velocities were measured using a pitot static probe, which leads to some uncertainties in the accuracy of the values immediately downstream of the hole, where the disturbances caused by the injected flow are strong.

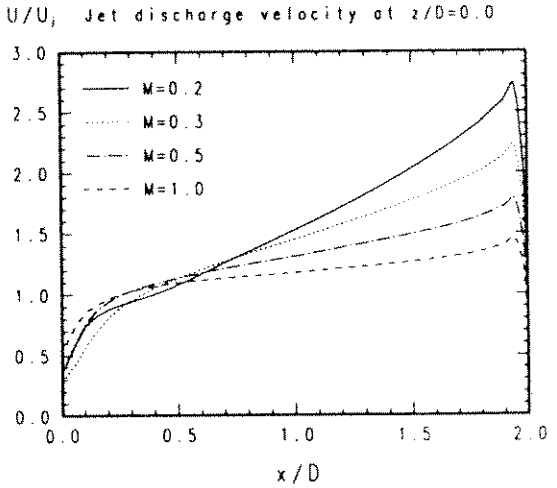

Figure 3. Mean velocity distribution across the jet-discharge plane at z/D=0.0 for different ratios of M.

The point $(x, y, z) = (0, 0, 0)$ in the computational domain, refers to the leading edge of the jet exit, see Fig. 1. The diameter of the hole is D=19.05 mm and the inlet boundary conditions for the free stream are set according to experiments and placed $7D$ upstream of the leading edge of the jet exit. Symmetry conditions are used through the center of the jet (at z/D=0.0) and at the opposite spanwise boundary (at z=5D). An upper symmetry boundary is placed at y=5D and the outlet boundary (x=25D downstream of the jet exit, where the streamwise derivatives are set to zero for all variables) is located sufficiently far downstream of the

jet exit, and hence the numerical results near the jet are believed not to be significantly influenced by these boundary conditions. Since it is not obvious how to determine the inlet boundary conditions for the jet at the hole exit (which are shown in Fig. 3 to be very non-uniform due to the influence by the free stream, especially in those cases where M is low), a fully developed turbulent flow is adopted at the jet inlet, which is placed approximately $6D$ upstream of the jet exit. The grid that is used in the calculations consists of $118\times72\times38$ grid points in the $x-$, $y-$ and $z-$direction respectively.

The velocity in the free stream is kept constant U_o=26 m/s, and by changing the velocity in the jet, different velocity ratios M are achieved. It should be noted that considering the adiabatic film-cooling effectiveness, the hot flow is in the jet and the cold flow is in the main stream. Due to the low concentration of the tracer gas within the jet flow, density variations are neglected in the calculations.

Fig. 4 shows how the streamwise mean velocity U varies with the distance y from the surface at various positions in the flow field when M=0.2, 0.5 and 1.0. At M=0.2, the influence by the jet on the free stream is generally very well predicted, although the profiles at the symmetry z/D=0.0 at the downstream positions x/D=4.20−5.80 in the wake region are slightly underpredicted, indicating that the recirculation zone just downstream of the jet exit is too large. When M=0.5, the deformation of the free stream is more pronounced, owing to the increased flow in the jet, which penetrates further away into the free stream. One may notice that along z/D=0.27 and z/D=0.53, the measured profiles in the wake region are more smeared out than the simulated ones, and that might indicate that in the calculations, the penetration of the high speed flow in the free stream into the wake region is too weak, and hence the mixing between the main stream and the jet flow is underpredicted. However, the simulations predict the local maximums and mininmums of the velocity profiles quite correctly. The local maximum of the velocity near the wall can be explained as follows. At larger values of M, the jet penetrates further into the mainstream, and the wake region in the lee of the jet is larger, associated with a lower local pressure. This causes an increased inflow in the spanwise direction towards the symmetry plane at z/D=0. This spanwise motion carries high-momentum fluid from the mainstream towards the symmetry plane and due to continuity this causes the maximum of the streamwise velocity near the wall as can be seen in the figure. When M=1.0, two local maximums in the velocity profiles can be seen. The upper one is probably owing to the fact that the streamwise velocity entering from the jet is higher than the velocity in the boundary layer of the crossflow.

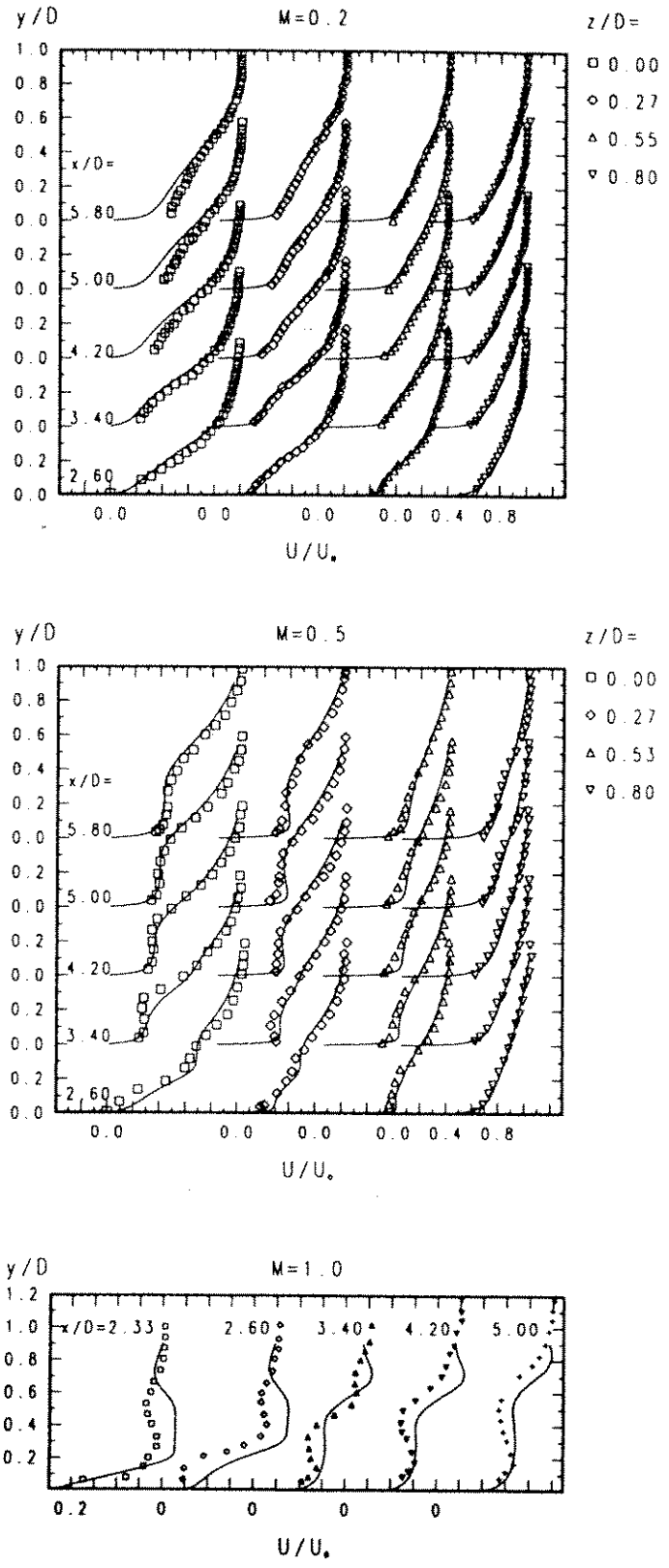

Figure 4. Predicted streamwise mean velocity distribution. Solid lines: predictions ($k-\epsilon$ model); markers: experiments.

The flow situation changes radically for the case when M=1.0, because of the jet's lifting away from the wall and the more rapid dilution rate associated with the increased penetration in all directions of the jet into the external fluid. There is a possibility that the flow field becomes unsteady in a small region just downstream of the jet, similar to vortex shedding behind a cylinder, since the strong jet might be affecting the crossflow as if it was a rigid obstacle. Then the mixing between the two flows will increase and the recirculation zone behind the jet exit will be reduced. This could then explain the poor predictions just behind the rear edge of the jet exit.

In Fig. 5, a full Reynolds stress model has been used to predict the streamwise mean velocities. At M=0.2, the simulated velocities are almost identical to those predicted by the $k-\epsilon$ model. In these cases, the separation region just behind the jet is very small, and hence the streamline curvature effects as well. At these lower values of M, the major contribution from the Reynolds stresses is that of $\overline{uv}$, and since $\overline{uv}$ is generally well predicted by the $k-\epsilon$ model, the predictions by both turbulence models become comparable. Hence, to take adequate account of production and pressure-strain effects of the individual Reynolds stresses is not important for the results of the mean flow at low values of M. However, at M=0.5, the flow in the jet penetrates further into the free stream, and greater curvature effects occur both in the streamwise and spanwise direction. Near the symmetry (z/D=0), where the streamline curvature effects are great, the velocity profiles are in slightly better agreement with the experiments than the predictions by the $k-\epsilon$ model. At the positions away from the symmetry in the spanwise direction, both turbulence models produce comparable results. At M=1.0, the predictions are still not in a very good agreement with the measurements.

The dependancy of the adiabatic film-cooling effectiveness Θ on the injection rate at various positions along the wall is also simulated. Θ can be expressed as:

$$\Theta = \frac{T_w - T_o}{T_j - T_o} \qquad (7)$$

where T_w is the wall temperature, T_o is the temperature in the crossflow and T_j is the temperature at the jet exit. In the present cases, the transport equation for the temperature consists of convection and diffusion only, and it can be written as:

$$\frac{\partial}{\partial x_j}(\rho U_j T) = \frac{\partial}{\partial x_j}\left(\mu\frac{\partial T}{\partial x_j} - \rho\overline{u_j\theta}\right) \qquad (8)$$

Since Θ is calculated using the temperature at the wall T_w, it is important to simulate the near-wall behaviour correctly. Close to the wall, the diffusion process in the normal direction is dominating, and the

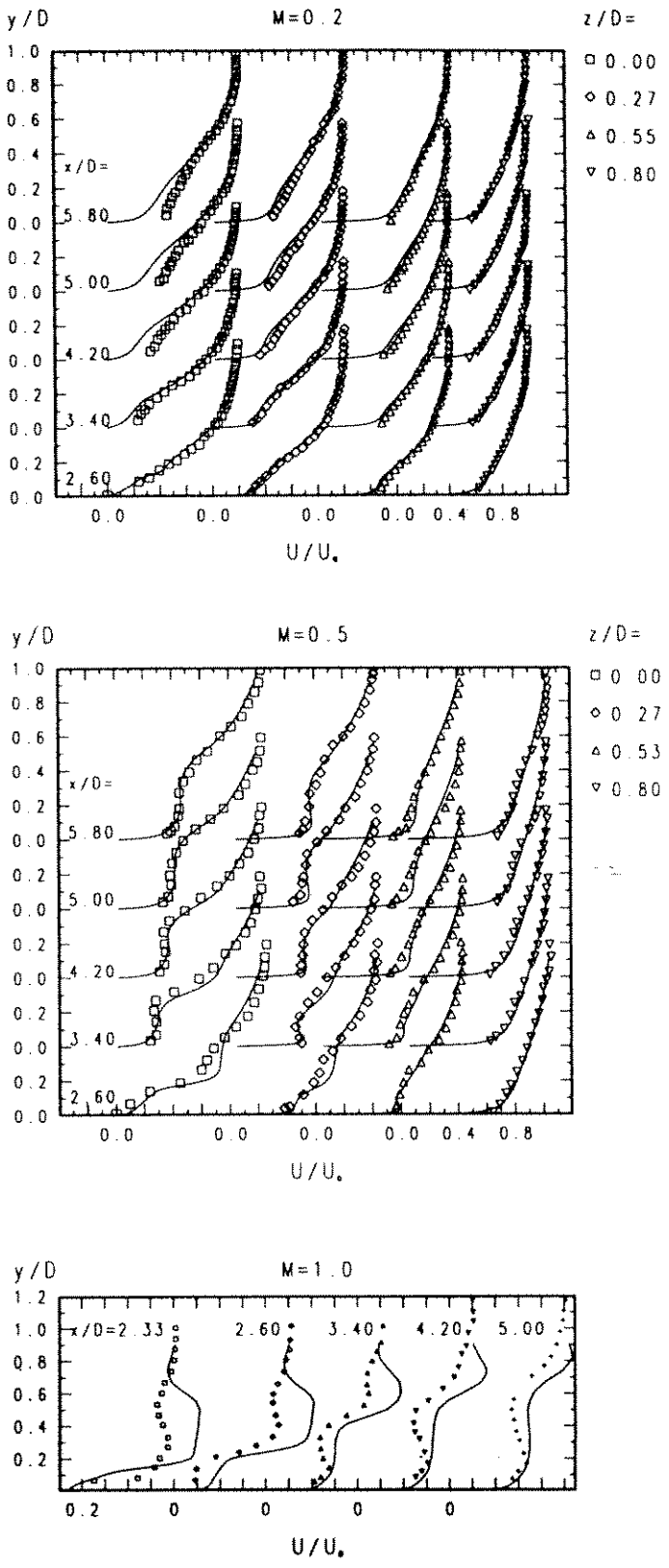

Figure 5. Predicted streamwise mean velocity distribution. Solid lines: predictions (RSM); markers: experiments.

value of T_w turned out to be extremely sensitive to how the turbulent heat flux $\overline{u_i\theta}$ is modelled in the near-wall region. The difficulty in modeling this turbulent heat flux is well established. When the $k-\varepsilon$ model was used, it was taken as:

$$-\rho\overline{u_j\theta} = \left(\frac{\mu_t}{Pr_t}\frac{\partial T}{\partial x_j}\right) \quad (9)$$

and when the RSM was used, this process was approximated by the following gradient-type expression:

$$-\rho\overline{u_j\theta} = \rho C_\theta \frac{k}{\varepsilon}\overline{u_iu_j}\frac{\partial T}{\partial x_i} \quad (10)$$

where the constant C_θ was taken as 0.11. However, close to the wall, where the transport equations for the Reynolds stresses are not valid, the turbulent heat flux was calculated from Eq. (9). At first, a constant value of the turbulent Prandtl number Pr_t (0.7–0.9) was used. There was a great difference between the obtained results of Θ, depending on the value of Pr_t, and the agreement with the measured film-cooling effectiveness was quite poor. However, it has been shown from direct numerical simulations by Kim and Moin [15] as well as from experiments by Blackwell [16], that the turbulent Prandtl number varies within the flow field, as can be seen in Fig. 6.

At high molecular Prandtl number flows, Pr_t is quite constant in the outer regions far away from a wall ($Pr_t \approx 0.85$), but it increases rapidly within the sublayer. An algebraic equation for the variation of Pr_t in a flow field can be found in Kays *et al.* [17]. The algebraic details are somewhat lengthy, so only the final result is presented here, in which Pr_t can be expressed as:

$$Pr_t = \frac{1}{C_1 + C\cdot C_2 - (C\cdot Pe_t)^2\cdot C_3} \quad (11)$$

where

$$C_1 = \frac{1}{2Pr_{t_\infty}}; \qquad C_2 = Pe_t\sqrt{\frac{1}{Pr_{t_\infty}}}$$

$$C_3 = \left[1 - exp\left(-\frac{1}{C\cdot Pe_t\sqrt{Pr_{t_\infty}}}\right)\right]$$

$Pe_t = (\mu_t/\mu)Pr$, Pr_{t_∞} is the value of Pr_t far from the wall (an experimental constant), and C is an experimental constant. The important point is that when the two free constants are specified by comparison with experiments, the final equation fits the available experimental data reasonably well, which is shown in Fig. 6. Eq. (11), with C=0.3 and Pr_{t_∞}=0.85, is plotted for the molecular Prandtl number Pr=0.7 (air). Note that it fits the experimental data for air quite well, including the rise of Pr_t in the sublayer.

In this study, Eq. (11) is used in order to describe the variation of Pr_t within the flow field. It should be pointed out that Eq. (11) in combination with a very high resolution of the grid near the wall (8-10 nodes within $y^+ \approx$10) turned out to be very important for the prediction of the near-wall behaviour. At first, a coarser grid was used (2 nodes within $y^+ \approx$10), but the temperatures at the wall were quite poorly predicted. One of the reasons might be the poorly predicted near-wall region of the flow. Hence, a very fine grid in this region is necessary to resolve the flow field, and thereby be able to predict the wall temperature more correctly.

The simulated distributions of film-cooling effectiveness are shown for different blowing rates. The effectiveness is plotted against the downstream distance (x/D) at various lateral locations. The results obtained by using the $k-\varepsilon$ model are shown in Fig. 7. A general trend at the blowing rates M=0.2–0.5, is that the effectiveness decays both along lines parallell to the line passing through the center of the hole in the streamwise direction, as well as along the adjacent lines in the spanwise direction. These effects are caused by the spreading of the jet into the mainstream and also by the mixing between the two flows. By increasing the value of M, both the level and the extent of the coverage increases and hence, a higher film-cooling effectiveness is achieved. When M=0.2, the predictions at x/D=0.0 are up to 25 % too high in the region close behind the jet exit and this may be explained by that the the spanwise motion of the crossflow in the leak of the jet towards the symmetry line is too weak. However, further downstream the effectiveness is better reproduced. The same conclusions can be drawn at x/D=0.27, although the overprediction of Θ in the region close to the hole is smaller (less than 10%). At x/D=0.54, the agreement with the experiments is quite good, but at x/D=0.80, the effectiveness is too low and hence the lateral spreading of the hot jet seems to be underpredicted. Increasing M to 0.5 these effects are even more pronounced and at this level of M, the streamline curvature effects become quite large in the region near the jet exit and hence the assumption of an isotropic character of the effective transport coefficients (turbulent diffusion) is quite crude. At M=1.0, Θ decreases radically, depending on that the jet is lifted entirely clear of the surface and the cold near-wall flow in the cross stream moves towards the spanwise symmetry downstream of the jet discharge. Although, the level of Θ is too high, the tendancy can be seen to be predicted in a correct way.

In Fig. 8, the corresponding distributions of the film-cooling effectiveness are shown when the RSM is used. Since the diffusion is the dominating process in the normal direction close to the wall, and this process is modelled the same way as when the $k-\varepsilon$ model is used, the predicted effectiveness is comparable to those ob-

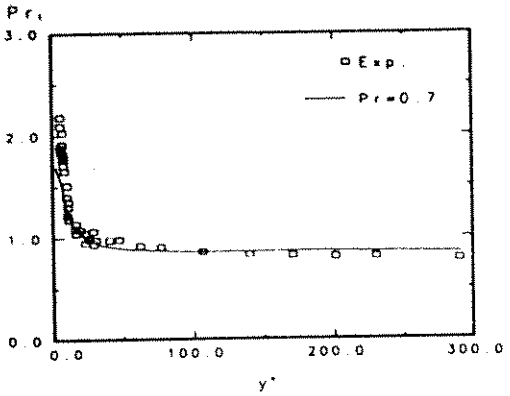

Figure 6. A plot of Eq. (11) for a boundary layer with no pressure gradient. The laminar Prandtl number is 0.7.

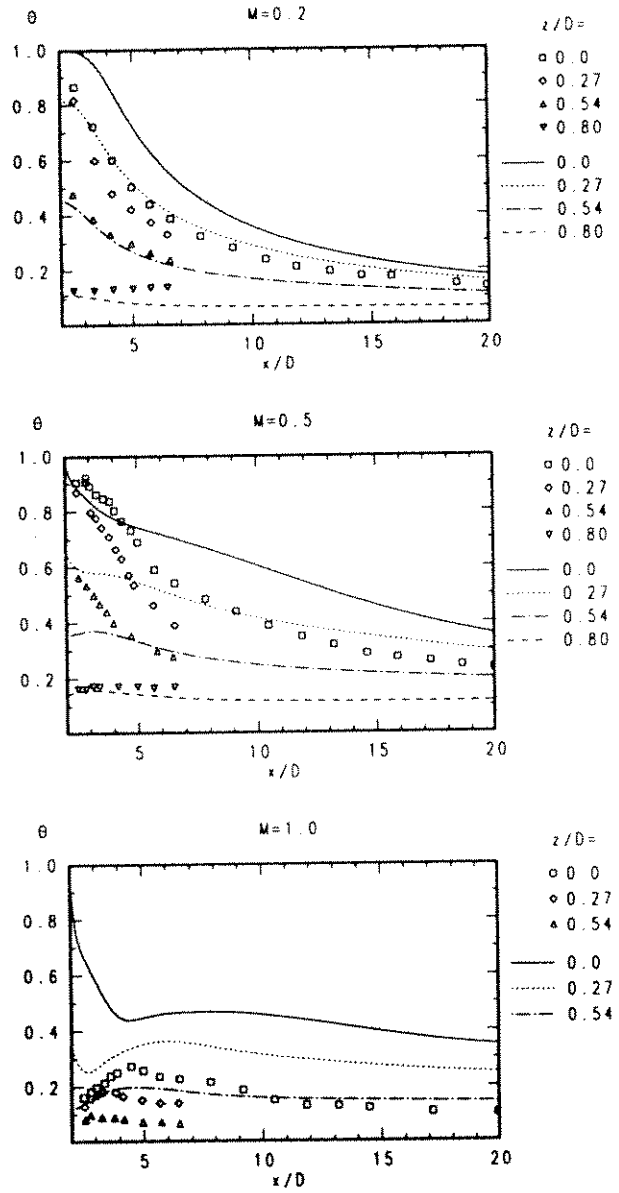

Figure 7. Adiabatic film-cooling effectiveness. Lines: predictions ($k-\epsilon$ model); markers: experiments.

tained by the $k-\epsilon$ model. However, at higher values of M and close behind the jet, where the convection becomes important in the direction normal to the wall, the predictions by the RSM are in slightly better agreement with the experiments. Obviously, it is important to model the turbulent heatflux in the near-wall region in a correct way, in order to describe the film-cooling effectiveness.

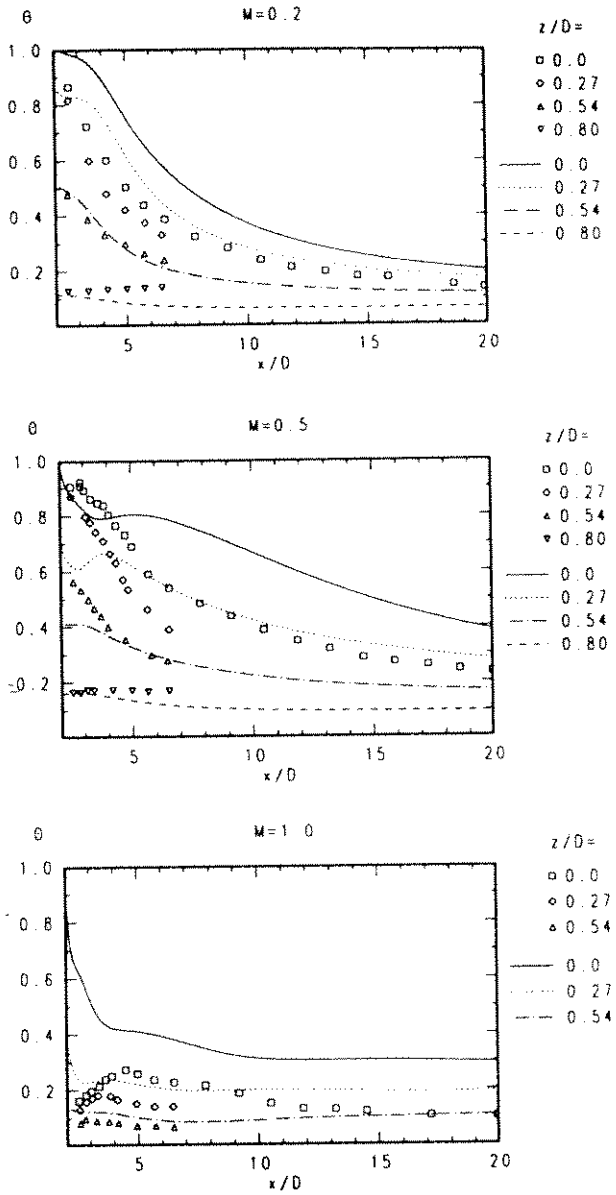

Figure 8. Adiabatic film-cooling effectiveness. Lines: predictions (RSM); markers: experiments.

6 CONCLUSIONS

In this study, numerical simulations have been carried out of a three-dimensional flow field associated with discrete-hole injection, with one single hole at an injection angle of 30° and at three different ratios of the in-

jection rate (M=0.2−1.0). Predicted streamwise mean velocities as well as the adiabatic film-cooling effectiveness have been compared to measurements by Bergeles *et al.* [3]. The following conclusions can be drawn:

- At lower values of the velocity ratio M=0.2−0.5, both turbulence models are capable of predicting the streamwise mean velocities very well. As M is increased, it is more important to take the anisotropic behaviour of the turbulence into account, and the RSM predicts the flow field slightly better than the $k-\epsilon$ model. At M=1.0 both models fail to reproduce the velocities correctly, possibly due to that the flow might exhibit an unsteady behaviour just downstream of the jet exit.
- Considering the film-cooling effectiveness Θ (or the temperatures at the wall T_w), both turbulence models produce similar results. The effectiveness close to the symmetry line passing through the center of the jet exit, is generally overpredicted, and away from the symmetry in the spanwise direction, the effectiveness is underpredicted. This indicates that the spreading of the jet is too small. The main reason to the difference between simulations and experiments is most likely due to the inadequate turbulence modelling in the near-wall region.

REFERENCES

[1] J. Andreopoulos and W. Rodi, 'Experimental Investigation of Jets in a Crossflow', *J. of Fluid Mech.*, **138**, 93-127, (1984).

[2] G. Bergeles, D. Gosman and B.E. Launder, 'The Near-field Character of a Jet Discharged Normal to a Mainstream', ASME *J. of Heat Transfer*, **98**, 373-378 (1976).

[3] G. Bergeles, D. Gosman and B.E. Launder, 'Near-field Character of a Jet Discharged Through a Wall at 30° to a Mainstream', *AIAA Journal*, **15**, 499-504, (1977).

[4] W.O. Afejuku, N. Hay and D. Lampard, 'Measured Coolant Distributions Downstream of Single and Double Rows of Film-Cooling Holes', ASME *J. of Engineering for Power*, **105**, 172-177 (1983).

[5] R.W. Claus and S.P. Vanka, 'Multigrid Calculations of a Jet in Crossflow', AIAA Paper 90-0444, (1990).

[6] S.W. Kim and T.J. Benson, 'Calculation of a Circular Jet in Crossflow with a Multiple-time-scale Turbulence Model', *Int. J. Heat Mass Transfer*, 2357-2365, (1992).

[7] N.Z. Ince and M.A. Leschziner, 'Calculation of Single and Multiple Jets in Crossflow with and without Impingement Using Reynolds-stress-transport Closure', AGARD Symp. on Computational and Experimental Assessment of Jets in Crossflow, Winchester, UK, April 1993.

[8] M. M. Gibson and B.E. Launder, 'Ground Effects on Pressure Fluctuations in the Atmospheric Boundary Layer', *J. Fluid Mech.*, **86**, 491-511, (1978).

[9] L.H. Norris and W.C. Reynolds, 'Turbulent Channel Flow with a Moving Wavy Boundary', Rept. No. FM-10, Dept. Mech. Eng., Stanford University, (1975).

[10] L. Davidson and B. Farhanieh, 'CALC-BFC: A Finite-Volume Code Employing Collocated Variable Arrangement and Cartesian Velocity Components for Computation of Fluid Flow and Heat Transfer in Complex Three-dimensional Geometries', Rept. 92/4, Dept. of Applied Thermodynamics and Fluid Mechanics, Chalmers Univ. of Tech., Gothenburg, (1989).

[11] B. van Leer, 'Towards the Ultimate Conservative Difference Scheme. Monotonicity and Conservation Combined in a Second Order Scheme', *J. Comp. Phys.*, **14**, 361-370, (1974).

[12] V.C. Patel, W. Rodi and G. Scheurer, 'Turbulence Models for Near-wall and Low-Reynolds Number Flows: A Review', *AIAA J.*, **23**, 1308-1319, (1985).

[13] P.G. Huang and M.A. Leschziner, 'Stabilization of Recirculating Flow Computations Performed with Second-moment Closures and Third-order Discretization', *Proc. 5th Symp. Turbulent Shear Flows*, 20.7-20.12, Cornell University, (1985).

[14] F.S. Lien and M.A. Leschziner, 'Second-moment Modelling of Recirculating Flow with a Non-orthogonal Collocated Finite-volume Algorithm', *Turbulent Shear Flows 8*, Springer Verlag, Berlin, 431, (1993).

[15] J. Kim and P. Moin, *Proceedings of 6th Symposium on Turbulent Shear Flows*, 5-2-1−5-2-6, September 7-9, Toulouse, (1987).

[16] B.F. Blackwell, W.M. Kays and R.J. Moffat, Report HMT-5, Thermosciences Division, Department of Mechanical Engineering, Stanford University, April 1969.

[17] W.M. Kays and M.E. Crawford, 'Convective Heat and Mass Transfer', McGraw-Hill, New York, (1993).